

Generating Multi-Scroll Chua's Attractors via Simplified Piecewise-Linear Chua's Diode

Ning Wang, Han Bao, Chengqing Li, Mo Chen, Bocheng Bao

Abstract—High implementation complexity of multi-scroll circuit is a bottleneck problem in real chaos-based communication. Especially, in multi-scroll Chua's circuit, the simplified implementation of piecewise-linear resistors with multiple segments is difficult due to their intricate irregular breakpoints and slopes. To solve the challenge, this paper presents a systematic scheme for synthesizing a Chua's diode with multi-segment piecewise-linearity, which is achieved by cascading even-numbered passive nonlinear resistors with odd-numbered ones via a negative impedance converter (NIC). As no extra DC bias voltage is employed and the scheme can be implemented by much simpler circuit. The voltage-current characteristics of the obtained Chua's diode are analyzed theoretically and verified by numerical simulations. Based on an available Chua's diode and a second-order active Sallen-Key high-pass filter, a new inductor-free Chua's circuit is then constructed to generate multi-scroll chaotic attractors. The circuit simulations and hardware experiments both confirmed the feasibility of the designed system.

Index Terms—Chaos, Chua's diode, Chua's circuit, multi-scroll chaotic attractor, Secure communication.

I. INTRODUCTION

SINCE Leon O. Chua proposed the first third-order autonomous chaotic oscillator and investigated systems owning double scrolls in 1980's [1], [2], the study of design, dynamics analysis and implementation of chaotic system have been received intensive attentions from the researchers in the field of nonlinear sciences and chaotic cryptography [3]–[10]. The subtle similarities between dynamics of chaotic system and the basic requirements of a secure cryptosystem also promoted research of the topic [11], [12]. Using all kinds of enhancing or controlling methods, the systems with various topological properties were obtained in the past two decades: multi-scroll attractors [13], multi-wing chaotic system [14]–[16], hyperchaotic system [17], multi-wing chaotic attractors [18]–[21] and hyperchaotic attractors [22]–[24] were also reported continually, which enriched the chaotic attractors with complex. Owing to the simple circuit structure and physical feasibility of Chua's circuit, it is considered as a prototype

This work was supported by the National Natural Science Foundation of China under Grant Nos. 51777016, 61601062, 61705021, 11602035, 51607013, 61532020, and 61772447, and the Natural Science Foundations of Jiangsu Province, China under Grant No. BK20160282.

N. Wang, H. Bao, M. Chen, and B. Bao are with the School of Information Science and Engineering, Changzhou University, Changzhou 213164, China (e-mail: cczuwangning@163.com, hi@charlesbao.com, mchen@cczu.edu.cn, mervinbao@126.com).

C. Li is with the School of Computer Science and Electronics Engineering, Hunan University, Changsha 410082, China (e-mail: DrChengqingLi@gmail.com).

for investigating multi-scroll attractors and other nonlinear systems.

Generally, multi-scroll Chua's attractors can be generated by adding additional saddle-focus-type equilibrium points. A typical approach is to use special nonlinear functions to reform the voltage-current characteristic of Chua's diode [2]. In earlier 1990's, Suykens and Vandewalle designed the first n -double scroll Chua's attractors by using a so-called quasi-linear function [25], [26]. In 1997, Suykens *et al.* proposed a more complete family of n -scroll Chua's attractors with the piecewise-linear function [27]. However, among these works, only numerical simulations were performed to verify existence of the multi-scroll attractors. In 2000, Yalçın *et al.* presented the circuit implementation of 3- and 5-scroll attractors from a generalized Chua's circuit [28]. Adopting a sine or cosine function, Tang *et al.* modified Chua's circuit to generate chaotic attractors owning 6 \sim 9 scrolls [29]. By using multi-segment piecewise-linear Chua's diode, Zhong *et al.* proposed a systematic approach to generate multiple-scroll Chua's attractors owning up to 10 scrolls [30]. Yu *et al.* presented an improved design approach for generating Chua's attractors with much more scrolls [31]. Especially, the sizes of the obtained scrolls with the method proposed in [31] are uniform. In 2007, Yu *et al.* further extended their methods to generate $n \times m$ -scroll attractors from a *single* Chua's circuit using a sawtooth function and a staircase function [32]. Multi-direction multi-double-scroll Chua's attractors can be obtained by constructing pulsed excitation in the direction, plane, and space of the corresponding state variable [33]. In [34], Wang *et al.* generated multi-scroll attractors from memristive Chua's circuit by introducing memristors with multi-piecewise continuous memductance function. In [35], a parametrically controlled method was used to generate multi-scroll Chua's attractors.

The implementation complexities of the above reviewed construction methods of multi-scroll attractors vary in a large range. Some of them involve a large number of discrete components [30], [31], [34], [35], extra DC bias voltages [20], [23], [30], [34], [35], or pulse excitations [21], [33], [36]. Such elements inevitably lead to complex selection of parasitic parameters, waste of hardware resources and cost of a large amount of energy. However, low-power consumption and facilitation is the basic requirement in some application scenarios, e.g. IoT devices and wireless communication. What's more, the electronic circuit with manually winding inductor element is bulky in terms of size and unsuitable for IC design.

To address the challenges, some inductor-free Chua's circuits were designed, e.g. inductance simulator based on general impedance converter [37], Chua's circuit based on electronic analogy [38], Chua's circuit based on Wien bridge oscillator [39] and Chua's circuit variants based on active band pass filter [40], [41].

This paper focuses on two points: 1) simplifying the implementation of multi-piecewise Chua's diode and providing a systematic way to determine element parameters; 2) extending the multi-scroll and inductor-free Chua's circuit family. As Chua's diode is the part of Chua's circuit consuming most energy of the whole system, changing its generation mechanism is an effective way to obtain multi-scroll with low circuit complexity. By modifying the implementation of Chua's diode, Bao *et al.* reported the coexisting multiple attractors [42] and hidden attractors [43] in Chua's circuit. Note that the saturation characteristic of op-amp is critical for the formulation of 3-segment piecewise-linear Chua's diode [2], [42], [43]. Obviously, the cascading combination of multiple piecewise-linear resistors is a approach for constructing multi-segment piecewise-linear Chua's diode. Based on this idea, we developed a novel scheme for implementing a multi-segment piecewise-linear Chua's diode and an inductor-free multi-scroll Chua's circuit. Both theoretical analyses and experimental simulations were provided to validate desired performances of the modified Chua's system.

The remainder of the paper is organized as follows. In Sec. II, we introduce a design method for implementing a multi-segment piecewise-linear Chua's diode. A third-order inductor-free Chua's circuit based on active Sallen-Key high-pass filter (HPF) is designed in Sec. III. The hardware experiment results of the design are provided in Sec. IV using Multisim circuit simulations. The last section concludes the paper.

II. SIMPLIFIED PIECEWISE-LINEAR CHUA'S DIODE

In this section, we first perform circuit syntheses of two types of nonlinear resistors, and then give a novel design scheme for implementing a simplified multi-segment piecewise-linear Chua's diode. Finally, two $v-i$ characteristics with 17 segments and 19 segments are presented.

A. Two Types of Nonlinear Resistors

The saturation characteristic of op-amp is considered to implement the 3-segment piecewise-linear resistor. Assume that the op-amp behaves a simplified characteristic without input offset voltage (VIO) between non-inverting and inverting input terminals and its input current $i_+ = i_- = 0$. The gain of the op-amp in the linear region tends to infinity. The op-amp is used to implement two types of op-amp based nonlinear resistors, named as passive 3-segment piecewise-linear resistor and active one, respectively. To facilitate description, the passive 3-segment piecewise-linear resistor is defined as type-I nonlinear resistor marked by N_{RI} and then the active 3-segment piecewise-linear resistor is defined as type-II nonlinear resistor marked by N_{RII} . Their schematic diagrams, element symbols, and voltage-current characteristic curves are plotted in Figs. 1 and 2, respectively.

1) *Type-I Passive Nonlinear Resistor*: The schematic diagram of the type-I passive nonlinear resistor is illustrated in Fig. 1(a), which contains one op-amp and two resistors and has the same circuit topology as the op-amp based gain circuit.

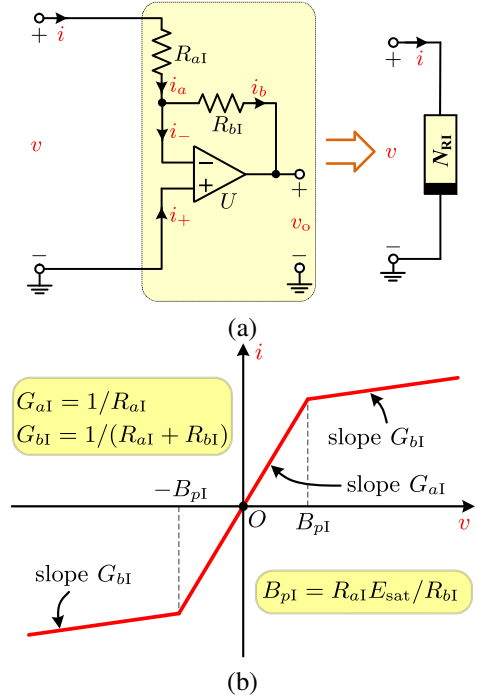


Fig. 1: Design of the type-I passive nonlinear resistor N_{RI} : (a) circuit implementation; (b) the $v-i$ characteristic curve.

By applying Kirchhoff's voltage and current laws, the voltage-current characteristic of N_{RI} can be classified as the following three cases:

- $|v| \leq B_{pI}$:
In this case, the op-amp works in a linear region. So, $\pm B_{pI} = \pm R_{aI} E_{sat} / R_{bI}$ are two breakpoints at both ends of the linear region. Then, one has $v_D = 0$, $i = (v - v_D) / R_{aI}$. Thus, the inner slope can be expressed as

$$G_{aI} = \frac{i}{v} = \frac{1}{R_{aI}}.$$

- $v > B_{pI}$:
The op-amp works in the negative saturation region and $v_o = -E_{sat}$. According to the current flowing through N_{RI} (i.e., the current passing R_{aI} and R_{bI}), one can get

$$\frac{v - v_D}{R_{aI}} = \frac{v_D - v_o}{R_{bI}}, \quad (1)$$

where $v_D \neq 0$. Then, one can obtain

$$v_D = \frac{R_{bI}v - R_{aI}E_{sat}}{R_{aI} + R_{bI}}. \quad (2)$$

Substituting (2) into (1), the current function related to the input voltage v can be presented as

$$i = f(v) = \frac{v + E_{sat}}{R_{aI} + R_{bI}}.$$

At the breakpoint, $B_{pI} = R_{aI}E_{\text{sat}}/R_{bI}$, $G_{aI}B_{pI} = E_{\text{sat}}/R_{bI}$. Thus, the outer slope can be expressed as

$$G_{bI} = \frac{\Delta i}{\Delta v} = \frac{f(v) - G_{aI}B_{pI}}{v - B_{pI}} = \frac{1}{R_{aI} + R_{bI}}.$$

- $v < -B_{pI}$:

Under this condition, the op-amp works in positive saturation region and $v_o = E_{\text{sat}}$, also, the outer slope can be derived as $G_{bI} = 1/(R_{aI} + R_{bI})$.

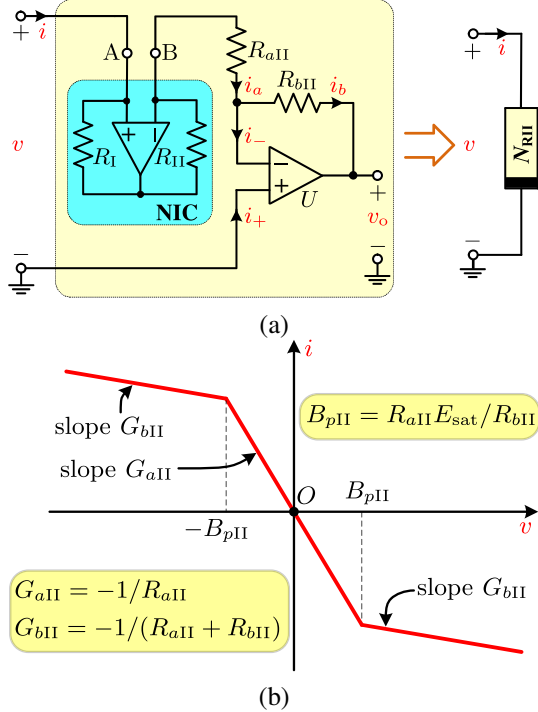


Fig. 2: Design of the type-II active nonlinear resistor N_{RII} : (a) circuit implementation; (b) the $v-i$ characteristic curve.

According to the above three cases, the $v-i$ characteristic of the N_{RI} is drawn as shown in Fig. 1(b), which can be featured by three parameters and represented as a uniform form

$$i = h(v) = G_{bI}v + 0.5(G_{aI} - G_{bI})(|v + B_{pI}| - |v - B_{pI}|).$$

where

$$G_{aI} = \frac{1}{R_{aI}}, G_{bI} = \frac{1}{R_{aI} + R_{bI}}, B_{pI} = \frac{R_{aI}E_{\text{sat}}}{R_{bI}}$$

denote the inner slope, outer slope, and breakpoint, respectively. As the three parameters satisfy $G_{aI} > 0$, $G_{bI} > 0$, and $G_{aI} > G_{bI}$, a passive three-segment piecewise-linear resistor is designed. It only occupies one op-amp and two resistors., the proposed type-I nonlinear resistor is the simplest op-amp-based piecewise-linear resistor.

2) *Type-II Active Nonlinear Resistor*: Linking a NIC to the input port of the N_{RI} , another type of active 3-segment piecewise-linear resistor can be obtained as shown in Fig. 2(a). The corresponding voltage-current characteristic of N_{RII} is shown in Fig. 2(b), which can be described as

$$i = h(v) = G_{bII}v + 0.5(G_{aII} - G_{bII})(|v + B_{pII}| - |v - B_{pII}|).$$

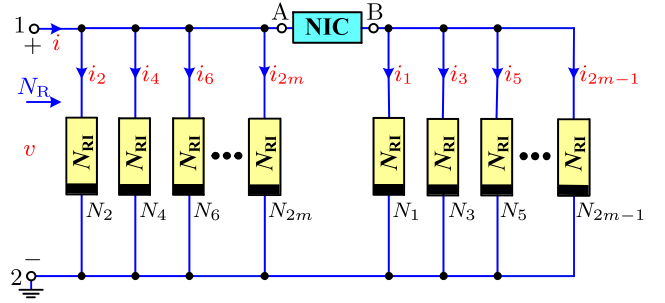


Fig. 3: The schematic of multi-piecewise Chua's diodes, where the m -th N_{RI} is marked as N_m .

where G_{aII} , G_{bII} , and B_{pII} are the inner slope, outer slope, and breakpoint, respectively. Observing Fig. 2, one can see that $G_{aII} < 0$, $G_{bII} < 0$, and $|G_{aII}| > |G_{bII}|$. When $R_I = R_{II}$, one has

$$G_{aII} = -\frac{1}{R_{aII}}, G_{bII} = -\frac{1}{R_{aII} + R_{bII}}, B_{pII} = \frac{R_{aII}E_{\text{sat}}}{R_{bII}}.$$

It can be seen that N_{RII} has the same characteristic as the classical Chua's diode with negative inner slope and outer slope. But, it employs fewer (four) resistors than the six ones in the classical Chua's diode designed in [2].

B. Multi-Segment Piecewise-Linear Chua's Diode

Adjusting the linear resistances of the equivalent circuit of N_{RI} , the inner slope, the outer slope and breakpoints can be freely adjusted. As shown in Fig. 3, a novel scheme for synthesizing the multi-segment piecewise-linear Chua's diode is proposed, where N_{RI} have the same inner slope but different breakpoints. Note that the NIC works as a current reverser here, which means that the odd-numbered N_{RI} work as type-II nonlinear resistors. Thus, the design scheme can also be regarded as the cascading combination of multiple N_{RI} and N_{RII} in turn.

As for the input voltage v and the input current i of the proposed Chua's diode, the voltage-current characteristic can be described as

$$i = h(v) = \sum_{m=1}^M (-1)^m [G_{bm}v + 0.5(G_{am} - G_{bm}) \times (|v + B_{pm}| - |v - B_{pm}|)], \quad (3)$$

where E_{sat} represents the op-amp saturation voltage, $G_{am} = 1/R_{am}$, $G_{bm} = 1/(R_{am} + R_{bm})$, and $B_{pm} = R_{am}E_{\text{sat}}/R_{bm}$ denote the inner slope, outer slope, and breakpoint of N_m , respectively.

Due to that one nonlinear resistor cell N_m can generate two symmetric breakpoints $\pm B_{pm}$, which is determined by resistance R_{am} , R_{bm} and op-amp saturation voltage E_{sat} . Thus, the cascading combination of M nonlinear resistor cells with different breakpoints can generate $2M + 1$ segments. Let $M-N_{RI}$ denotes the cascading combination of M -stage type-I nonlinear resistors, the parameters of $M-N_{RI}$ -based Chua's diode can be determined with the following steps:

- Keep the op-amp saturation voltage E_{sat} unchanged, and set the values of the outermost breakpoints $\pm B_{pI}$.

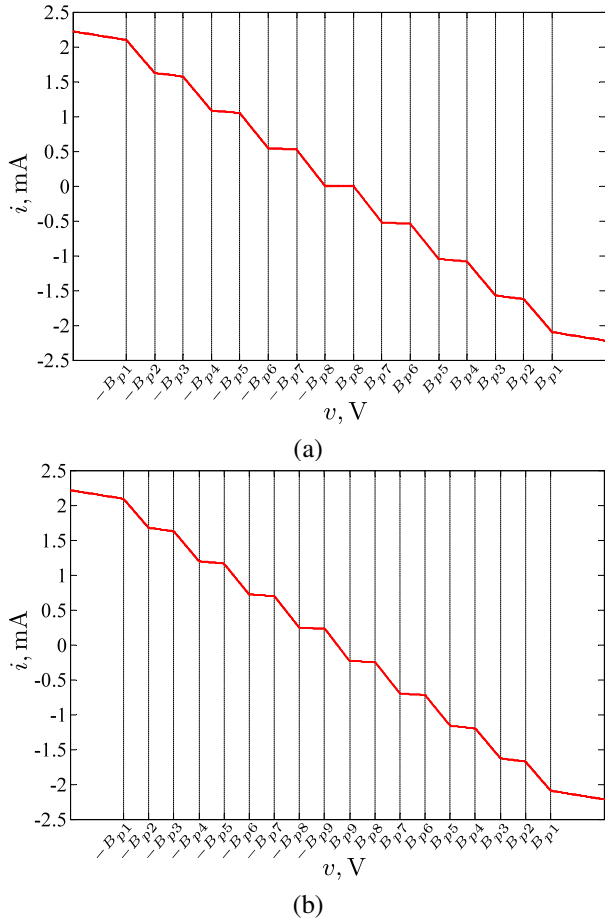


Fig. 4: The $v-i$ characteristics of the proposed Chua's diodes: (a) the 17-segment piecewise-linear curve; (b) the 19-segment piecewise-linear curve.

- Averagely divide the interval between $-B_{p1}$ and B_{p1} into $2M - 1$ segments. The breakpoints generated from N_m , R_{bm} , are calculated as

$$\pm B_{pm} = \pm \frac{2B_{p1}}{2M - 1} (M - m + 0.5),$$

where $m = 1, 2, \dots, M$.

- Fix the inner slope of N_{RI} , i.e., keep resistance $R_{a1} = R_{a2} = \dots = R_{aM}$ unchanged.
- Set

$$R_{bm} = \frac{R_{am}}{B_{pm}} E_{sat}.$$

C. The $v-i$ Characteristic of the Proposed Chua's Diode

To illustrate their $v-i$ characteristics of the proposed Chua's diodes, the 8- N_{RI} and 9- N_{RI} -based Chua's diodes ($M = 8, 9$) as used as two typical examples. The resistance R_{am} are fixed as $1 \text{ k}\Omega$ for $m = 1 \sim M$. In addition, the op-amp saturation output voltage $E_{sat} = 13 \text{ V}$ and the outermost breakpoints $\pm B_{p1} = \pm 4 \text{ V}$ are adopted. Using the parameter determination steps described in the above sub-section, two sets of element values are calculated and listed in Table I. The loci of the two Chua's diodes in the $v-i$ plane are plotted as shown in Fig. 4(a) and (b), which show 17 segments and 19 segments,

TABLE I: Element Values and Parameters of Chua's Diode.

M	Element values	Parameters of Chua's diode
8	$R_{ai} = 1 \text{ k}\Omega, i = 1 \sim 8$	$G_{ai} = 1 \text{ mS}, i = 1 \sim 8$
	$R_{b1} = 3.25 \text{ k}\Omega$	$G_{b1} = 235.294 \text{ }\mu\text{S}, B_{p1} = 4 \text{ V}$
	$R_{b2} = 3.75 \text{ k}\Omega$	$G_{b2} = 210.526 \text{ }\mu\text{S}, B_{p2} = 52/15 \text{ V}$
	$R_{b3} = 4.432 \text{ k}\Omega$	$G_{b3} = 184.094 \text{ }\mu\text{S}, B_{p3} = 44/15 \text{ V}$
	$R_{b4} = 5.417 \text{ k}\Omega$	$G_{b4} = 155.836 \text{ }\mu\text{S}, B_{p4} = 12/5 \text{ V}$
	$R_{b5} = 6.964 \text{ k}\Omega$	$G_{b5} = 125.565 \text{ }\mu\text{S}, B_{p5} = 28/15 \text{ V}$
	$R_{b6} = 9.75 \text{ k}\Omega$	$G_{b6} = 93.023 \text{ }\mu\text{S}, B_{p6} = 4/3 \text{ V}$
	$R_{b7} = 16.25 \text{ k}\Omega$	$G_{b7} = 57.971 \text{ }\mu\text{S}, B_{p7} = 3/5 \text{ V}$
	$R_{b8} = 48.75 \text{ k}\Omega$	$G_{b8} = 20.101 \text{ }\mu\text{S}, B_{p8} = 4/15 \text{ V}$
9	$R_{aj} = 1 \text{ k}\Omega, j = 1 \sim 8$	$G_{aj} = 1 \text{ mS}, j = 1 \sim 8$
	$R_{b1} = 3.25 \text{ k}\Omega$	$G_{b1} = 235.294 \text{ }\mu\text{S}, B_{p1} = 4 \text{ V}$
	$R_{b2} = 3.683 \text{ k}\Omega$	$G_{b2} = 213.538 \text{ }\mu\text{S}, B_{p2} = 60/17 \text{ V}$
	$R_{b3} = 4.25 \text{ k}\Omega$	$G_{b3} = 190.476 \text{ }\mu\text{S}, B_{p3} = 52/17 \text{ V}$
	$R_{b4} = 5.023 \text{ k}\Omega$	$G_{b4} = 166.030 \text{ }\mu\text{S}, B_{p4} = 44/17 \text{ V}$
	$R_{b5} = 6.139 \text{ k}\Omega$	$G_{b5} = 140.076 \text{ }\mu\text{S}, B_{p5} = 36/17 \text{ V}$
	$R_{b6} = 7.893 \text{ k}\Omega$	$G_{b6} = 112.448 \text{ }\mu\text{S}, B_{p6} = 28/17 \text{ V}$
	$R_{b7} = 11.05 \text{ k}\Omega$	$G_{b7} = 82.988 \text{ }\mu\text{S}, B_{p7} = 20/17 \text{ V}$
	$R_{b8} = 18.417 \text{ k}\Omega$	$G_{b8} = 51.501 \text{ }\mu\text{S}, B_{p8} = 12/17 \text{ V}$
	$R_{b9} = 55.25 \text{ k}\Omega$	$G_{b9} = 17.778 \text{ }\mu\text{S}, B_{p9} = 4/17 \text{ V}$

respectively. Considering that a NIC based current reverser is necessary, the two examples can be also named as 9-stage and 10-stage op-amp-based Chua's diodes, respectively.

Comparing with the construction approach of n -scroll attractor in [30], all extra DC bias voltages are removed in the proposed approach. Meanwhile, fewer resistors are employed for generating the same number of segments. Taking 17 segments as an example, the proposed Chua's diode employs 18 resistors. In contrast, the numbers required in [30] and [31] are 27 and 48, respectively.

III. SALLEN-KEY HPF-BASED CHUA'S CIRCUIT

In this section, a third-order inductor-free Chua's circuit is designed to generate multi-scroll chaotic attractors using an available Chua's diode.

A. Circuit Description and State Equation

As shown in Fig. 5, a new inductor-free Chua's circuit can be constructed by replacing the parallel connection LC network in the classical Chua's circuit with a second-order active Sallen-Key high-pass filter (HPF) designed in [44]. The proposed Chua's diode is placed in the right part of the ports "1" and "2". Meanwhile, a second-order Sallen-Key HPF is set in the left part of the ports "3" and "4". In the Sallen-Key HPF, $C_2 = C_3$ and $R_3 = R_4$. Comparing with the Wien bridge oscillator [39], second-order active band pass filter [40], [41], and second-order active Sallen-Key low-pass filter [45], the Sallen-Key HPF has the same off-the-shelf discrete components but different circuit structures.

The circuit shown in Fig. 5 is a third-order autonomous circuit containing three dynamical elements of capacitor C_1 , C_2 , and C_3 , which can be featured by three coupled first-order autonomous differential equations in terms of three node

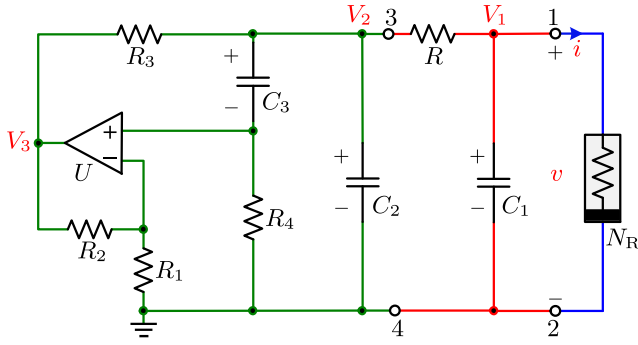


Fig. 5: Schematic of the Sallen-Key HPF-based Chua's circuit.

voltages of V_1 , V_2 , and V_3 ,

$$\begin{cases} \frac{dV_1}{dt} = -\frac{V_1 - V_2}{RC_1} - \frac{h(V_1)}{C_1}, \\ \frac{dV_2}{dt} = \frac{V_1 - V_2}{RC_2} + \frac{(k-1)V_3 - kV_2}{kR_3C_2}, \\ \frac{dV_3}{dt} = \frac{k(V_1 - V_2)}{RC_3} + \frac{(k-2)V_3 - kV_2}{R_3C_3}, \end{cases} \quad (4)$$

where $k = 1 + R_2/R_1$, and $h(V_1)$ expressed by Eq. (3) stands for the voltage-current characteristic of the Chua's diode.

B. Equilibrium Point and Its Stability

Let $\frac{dV_1}{dt} = 0$, it is easy to obtain

$$V_2 = V_1 + Rh(V_1). \quad (5)$$

If $\frac{dV_2}{dt}$ and $\frac{dV_3}{dt}$ are both equal to zero, one can obtain $V_3 = 0$, and

$$V_2 = R_3V_1/(R + R_3). \quad (6)$$

Thus, the solutions of V_1 and V_2 are the intersection points of the two curves measured by Eq. (5) and (6).

The linear element parameters of the circuit shown in Fig. 5 are configured as follows: $R = 1.5 \text{ k}\Omega$, $R_1 = 3 \text{ k}\Omega$, $R_2 = 6.6 \text{ k}\Omega$, $R_3 = R_4 = 500 \text{ }\Omega$, $C_1 = 6.8 \text{ nF}$, and $C_2 = C_3 = 100 \text{ nF}$. When the parameters listed in Table I are utilized for the 8- N_{RI} and 9- N_{RI} -based Chua's diodes ($M = 8, 9$), the two functions 5) and (6) are simultaneously plotted in Fig. 6(a) and (b), respectively, where Eq. (5) is coloured in red and marked as h_1 , and Eq. (6) is coloured in blue and marked as h_2 . As there are $(2M+1)$ intersection points generated from the inductor-free Chua's circuit with M - N_{RI} based Chua's diode, all equilibrium points can be calculated, as listed in Table II.

The Jacobian matrix corresponding to every equilibrium point is

$$\mathbf{J} = \begin{bmatrix} -\frac{1}{RC_1} - \frac{H(V_1)}{C_1} & \frac{1}{RC_1} & 0 \\ \frac{1}{RC_2} & -\frac{R + R_3}{RR_3C_2} & \frac{k-1}{kR_3C_2} \\ \frac{k}{RC_3} & -\frac{k(R + R_3)}{RR_3C_3} & \frac{k-2}{R_3C_3} \end{bmatrix} \quad (7)$$

where

$$H(V_1) = \sum_{m=1}^M (-1)^m \{G_{bm} + 0.5(G_{am} - G_{bm}) \cdot [\text{sgn}(V_1 + B_{pm}) - \text{sgn}(V_1 - B_{pm})]\}.$$

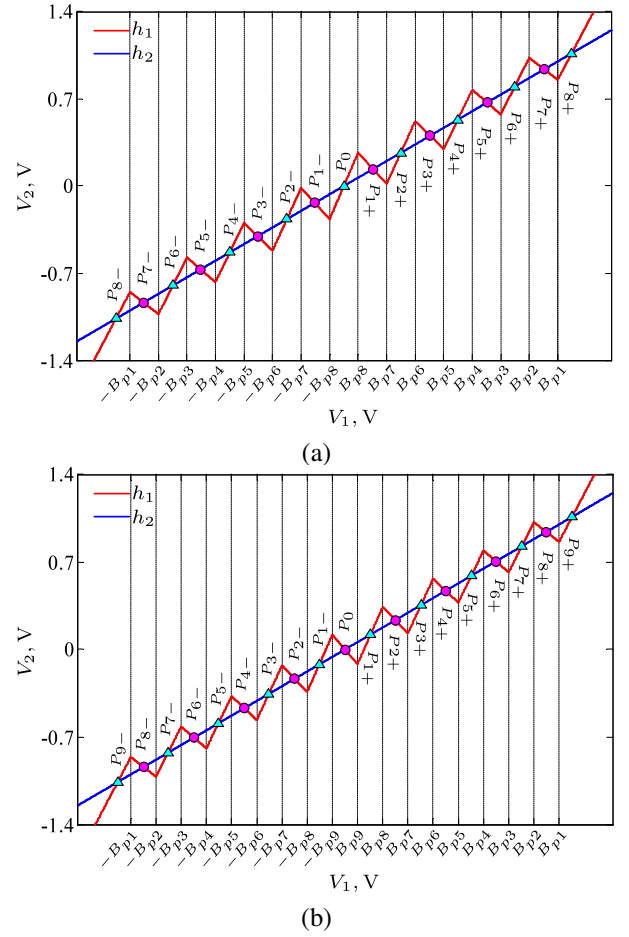


Fig. 6: Equilibrium points in the $V_1 - V_2$ plane: (a) Chua's circuit owing 17 equilibrium points. (b) Chua's circuit owing 19 equilibrium points, where the index-1 saddle-foci are marked by magenta circles and the index-2 saddle-foci are marked by cyan triangles.

As for the Jacobian matrices at the equilibrium points, the corresponding eigenvalues are listed in Table II. Observing Table II, one can see that the equilibrium points can be divided into two classes: 1) unstable index-1 saddle-foci owning a positive real root and two complex conjugate roots with negative real parts; 2) unstable index-2 saddle-foci owning two complex conjugate roots with positive real parts and a negative real root. Consequently, as for the inductor-free Chua's circuit with 8- N_{RI} based Chua's diode ($M = 8$), there exists eight unstable index-1 saddle-foci, $P_{1\pm}$, $P_{3\pm}$, $P_{5\pm}$, $P_{7\pm}$, and nine unstable index-2 saddle-foci, P_0 , $P_{2\pm}$, $P_{4\pm}$, $P_{6\pm}$, $P_{8\pm}$. As for the inductor-free Chua's circuit with 9- N_{RI} based Chua's diode ($M = 9$), there exists nine unstable index-1 saddle-foci, P_0 , $P_{2\pm}$, $P_{4\pm}$, $P_{6\pm}$, $P_{8\pm}$, and ten unstable index-2 saddle-foci, $P_{1\pm}$, $P_{3\pm}$, $P_{5\pm}$, $P_{7\pm}$, $P_{9\pm}$.

According to Shil'nikov theorem given in [46], chaos may emerge in a system if there are one real root γ and two complex conjugate roots $\sigma \pm j\omega$ satisfying $|\frac{\sigma}{\gamma}| < 1$ and $\sigma\gamma < 0$ among the eigenvalues of its equilibrium points. When suitable configuration parameters are adopted, the corresponding bond orbits and scrolls may be generated in the neighborhoods of

TABLE II: Equilibrium Points and Corresponding Eigenvalues.

M	Equilibrium points	Eigenvalues	Types of equilibrium points
8	$P_0 : (0V, 0V, 0V)$	$\lambda_{1,2} = 1162 \pm j19475, \lambda_3 = -103030$	unstable index-2 saddle-focus
	$P_{1\pm} : (\pm 0.5445V, \pm 0.1361V, 0V)$	$\lambda_1 = 58532, \lambda_{2,3} = -7569 \pm j24202$	unstable index-1 saddle-foci
	$P_{2\pm} : (\pm 1.0653V, \pm 0.2663V, 0V)$	$\lambda_{1,2} = 1254 \pm j19226, \lambda_3 = -97644$	unstable index-2 saddle-foci
	$P_{3\pm} : (\pm 1.6118V, \pm 0.4029V, 0V)$	$\lambda_1 = 54299, \lambda_{2,3} = -8029 \pm j24043$	unstable index-1 saddle-foci
	$P_{4\pm} : (\pm 2.1308V, \pm 0.5327V, 0V)$	$\lambda_{1,2} = 1336 \pm j18985, \lambda_3 = -93024$	unstable index-2 saddle-foci
	$P_{5\pm} : (\pm 2.6786V, \pm 0.6696V, 0V)$	$\lambda_1 = 50719, \lambda_{2,3} = -8464 \pm j23863$	unstable index-1 saddle-foci
	$P_{6\pm} : (\pm 3.1962V, \pm 0.7991V, 0V)$	$\lambda_{1,2} = 1411 \pm j18751, \lambda_3 = -89017$	unstable index-2 saddle-foci
	$P_{7\pm} : (\pm 3.7463V, \pm 0.9366V, 0V)$	$\lambda_1 = 47655, \lambda_{2,3} = -8876 \pm j23655$	unstable index-1 saddle-foci
	$P_{8\pm} : (\pm 4.2615V, \pm 1.0654V, 0V)$	$\lambda_{1,2} = 1477 \pm j18526, \lambda_3 = -85508$	unstable index-2 saddle-foci
9	$P_0 : (0V, 0V, 0V)$	$\lambda_1 = 61005, \lambda_{2,3} = -7326 \pm j24273$	unstable index-1 saddle-focus
	$P_{1\pm} : (\pm 0.4793V, \pm 0.1198V, 0V)$	$\lambda_{1,2} = 1205 \pm j19362, \lambda_3 = -100501$	unstable index-2 saddle-foci
	$P_{2\pm} : (\pm 0.9402V, \pm 0.2351V, 0V)$	$\lambda_1 = 56878, \lambda_{2,3} = -7742 \pm j24146$	unstable index-1 saddle-foci
	$P_{3\pm} : (\pm 1.4209V, \pm 0.3552V, 0V)$	$\lambda_{1,2} = 1282 \pm j19144, \lambda_3 = -96026$	unstable index-2 saddle-foci
	$P_{4\pm} : (\pm 1.8804V, \pm 0.4701V, 0V)$	$\lambda_1 = 53342, \lambda_{2,3} = -8141 \pm j24000$	unstable index-1 saddle-foci
	$P_{5\pm} : (\pm 2.3625V, \pm 0.5906V, 0V)$	$\lambda_{1,2} = 1353 \pm j18933, \lambda_3 = -92105$	unstable index-2 saddle-foci
	$P_{6\pm} : (\pm 2.8204V, \pm 0.7051V, 0V)$	$\lambda_1 = 50285, \lambda_{2,3} = -8520 \pm j23839$	unstable index-1 saddle-foci
	$P_{7\pm} : (\pm 3.3045V, \pm 0.8261V, 0V)$	$\lambda_{1,2} = 1418 \pm j18728, \lambda_3 = -88639$	unstable index-2 saddle-foci
	$P_{8\pm} : (\pm 3.7612V, \pm 0.9403V, 0V)$	$\lambda_1 = 47615, \lambda_{2,3} = -8881 \pm j23662$	unstable index-1 saddle-foci
$P_{9\pm} : (\pm 4.2457V, \pm 1.0614V, 0V)$	$\lambda_{1,2} = 1476 \pm j18529, \lambda_3 = -85556$	unstable index-2 saddle-foci	

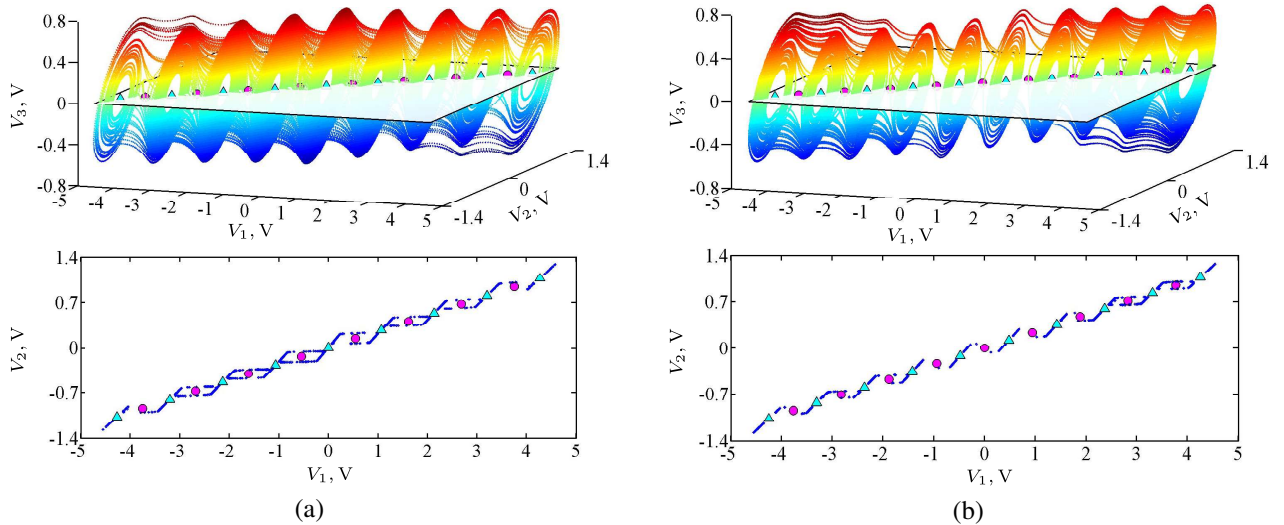


Fig. 7: Numerical simulation results of chaotic attractors: the upper panel of (a) the Poincaré section (upper panel) and the crossing Poincaré section of 9-scroll chaotic attractor; (b) the Poincaré section (upper panel) and the crossing Poincaré section of 10-scroll chaotic attractor.

unstable index-1 and index-2 equilibria, respectively.

C. Multi-Scroll Chaotic Attractor

To verify the above theoretical analyses, a large number of experiments were performed using Runge-Kutta algorithm (ODE45 in MATLAB) with time-step $1 \mu s$ and time-interval [10 ms, 200 ms]. When the initial conditions of three state variables are set as $(V_1(0), V_2(0), V_3(0)) = (0.1mV, 0V, 0V)$, the phase portraits and Poincaré map of a 9-scroll attractor and a 10-scroll one are plotted in Fig. 7(a) and (b), respectively. In Fig. 7, the unstable index-1 saddle-foci and unstable index-2 saddle-foci are marked by the symbols “•” and “▲”, respectively. It is found that the scrolls emerge from the neighbourhoods of unstable index-2 saddle-foci, while the bond orbits are generated from the neighbourhoods of unstable index-1 saddle-foci.

Generally, Poincaré map can be used to preliminarily distinguish the state of the motion: the crossing trajectory of

discrete points means the periodic state; the crossing trajectory of continuous curve means the chaotic state; the crossing trajectory of plane with no regular limbs implies the hyper-chaotic state. Considering the equilibrium points are always distributed in the $V_1 - V_2$ plane, the plane of $V_3 = 0$ is chosen as Poincaré section for better observation of locations of the scrolls and the state of the whole attractor. The projections of Poincaré map of the 9-scroll and 10-scroll chaotic attractors in the $V_1 - V_2$ plane are plotted, as shown in lower of Fig. 7(a) and (b), respectively. It can be easily observed that the continuous curve-like maps occur in the neighbourhoods of unstable index-2 saddle-foci, indicating the emergence of multi-scroll chaotic attractors.

In theory, the proposed method can construct $(2M + 1)$ -segment piecewise linear curve by adjusting the $3M$ parameters of the $M-N_{RI}$ -based Chua's diode. When suitable parameters are configured, $(M + 1)$ -scroll attractor can be coined from the Chua's circuit with the proposed Chua's diode.

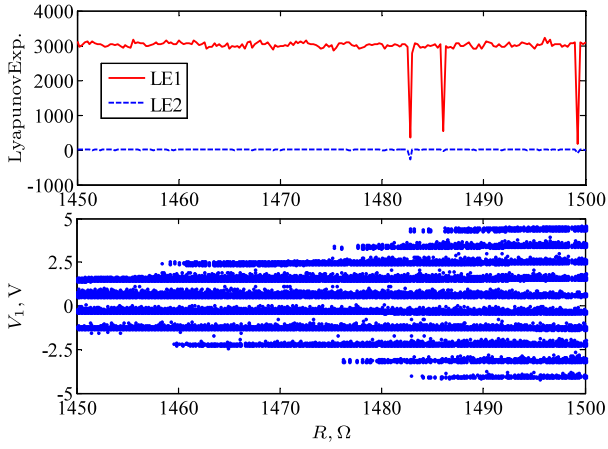


Fig. 8: The dynamical behavior with respect to R , where the upper panel depicts the first two Lyapunov exponents and the lower panel plots the bifurcation diagrams of the local maxima of V_1 .

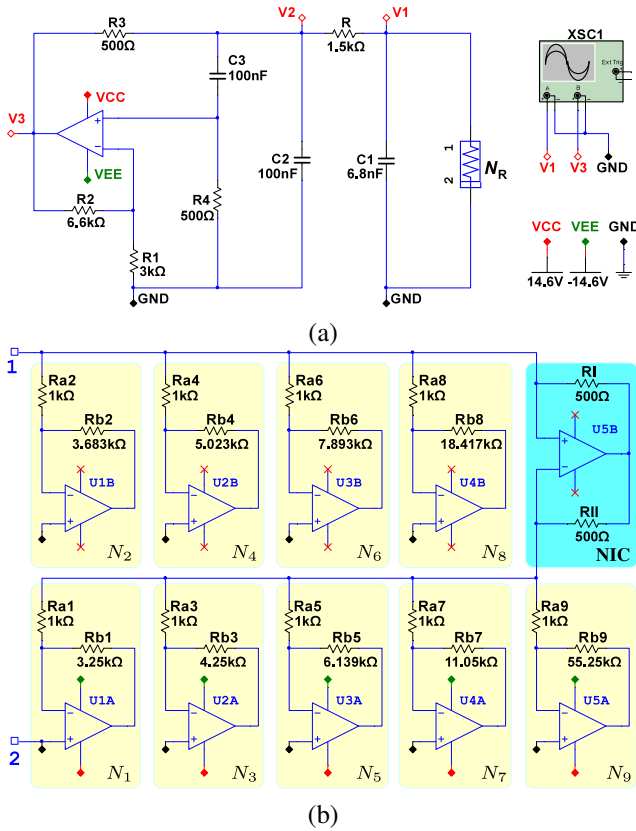


Fig. 9: Multisim circuit simulation model: (a) the Sallen-Key HPF-based inductor-free Chua's circuit; (b) the implementation of 9- N_{RI} -based Chua's diode.

D. Parameter-Dependent Bifurcation Behavior

To study dynamical behaviors of the proposed system, the Sallen-Key HPF-based Chua's circuit with various segment piecewise-linear Chua's diode were measured in terms of Lyapunov exponents and bifurcation diagram. When the resistance R is continuously changed from 1.45 k Ω to 1.5 k Ω , the first two finite time Lyapunov exponents calculated by Wolf's

method given in [47] and bifurcation diagram of the local maxima (denoted by V_1) of the state variable V_1 are plotted in Fig. 8. For the bifurcation diagram in Fig. 8, the trajectories are initiated from the initial conditions (0.1 mV, 0 V, 0 V). It is observed from Fig. 8 that there always exist positive largest Lyapunov exponents in the region of $R \in [1.45k\Omega, 1.5k\Omega]$, indicating emergence of chaos. Furthermore, dynamical behaviors including 4-, 6-, 8-, and 10-scroll chaotic attractors are observed.

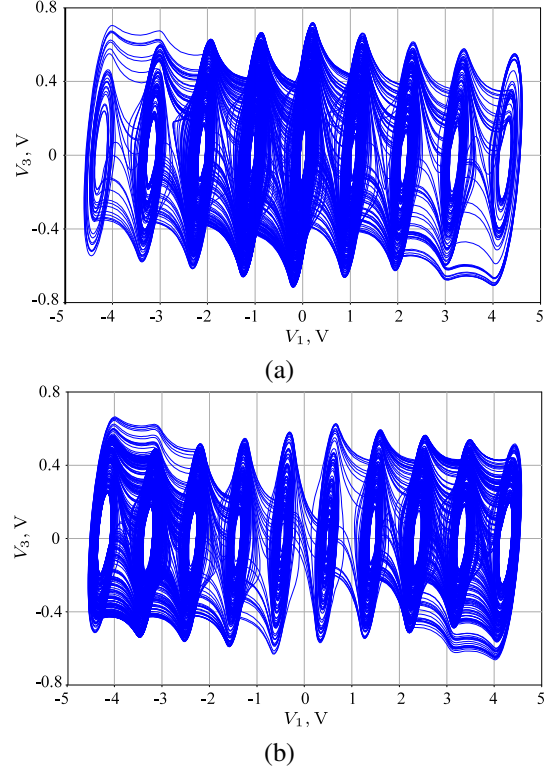


Fig. 10: Chaotic attractors simulated in circuit: (a) The 9-scroll chaotic attractor; (b) the 10-scroll chaotic attractor.

IV. CIRCUIT SIMULATIONS AND HARDWARE EXPERIMENTS

Circuit simulations and hardware experiments are necessary for circuit syntheses and verifications. Some regular circuit design and simulation software, for examples, Pspice [21], [33], [38], Multisim [19], [36], [41], and PSIM [43], [48], [49] can provide reliable operating environment for circuit simulations. In this section, the simulation results of the proposed system by Multisim circuit simulations and hardware experiments were described to verify its real performances.

A. Multisim Circuit Simulations

Using the circuit schematics shown in Figs. 3 and 5, the circuit simulation model of the Sallen-Key HPF-based Chua's circuit can be constructed using Multisim 12.0 simulation software. As a typical example, the Chua's circuit with 9- N_{RI} -based Chua's diode is given in Fig. 9. With the parameters of Chua's diode listed in Table I and the element parameters given in section III-B, the phase portraits in the $V_1 - V_3$

plane are simulated, as shown in Fig. 10(a) and (b), which just demonstrate the 9-scroll and 10-scroll Chua's chaotic attractors, respectively. It is observed that the simulation results with the Multisim circuit shown in Fig. 10 agree well with the numerical simulation results demonstrated in Fig. 7.

B. Hardware Experiments

Using the circuit simulation model in Fig. 9, the Sallen-Key HPF-based Chua's circuit with the simplified multi-segment piecewise-linear Chua's diode was performed on a hardware breadboard, where adjustable resistors, monolithic ceramic capacitors, and op-amps TL082CP with $\pm 14.6\text{V}$ DC power supplies ($E_{\text{sat}} \approx 13\text{V}$) were adopted. The snapshot of the hardware breadboard linked with a digital oscilloscope is shown in Fig. 11.

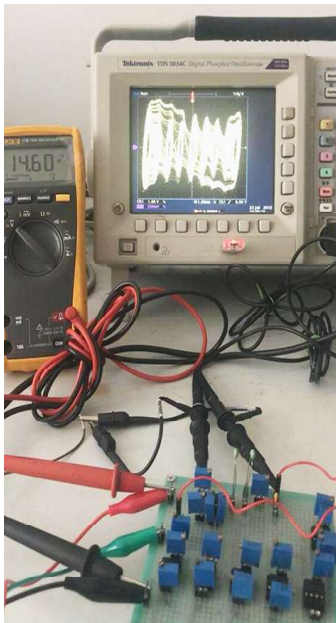


Fig. 11: Snapshot of the hardware experiment setup.

First, to verify the v - i characteristics of the proposed Chua's diode, the continuous sinusoidal signal $v_s = V_m \sin(2\pi ft)$ provided by Tektronix AFG3022 function generator was used for the driven voltage, and Tektronix TCP213A current probe was used to detect the input current. With Tektronix TDS3034C four-channel digital phosphor oscilloscope, the experimental results can be intuitively captured. When the continuous sinusoidal signal v_s is deployed as $V_m = 5\text{V}$ and $f = 100\text{Hz}$, the experimentally measured loci in the $v-i$ plane are shown in Fig. 12(a) and (b), respectively. Note that the experimental captured currents are measured by magnifying four times for better view. Furthermore, the phase portraits of 9-scroll and 10-scroll chaotic attractors in the V_1 - V_3 plane are experimentally measured, as shown in Fig. 12(c) and (d), respectively. Ignoring the deviations caused by parasitic circuit parameters, one can see that the circuit simulations and hardware experiments are both consistent well with that obtained in the numerical simulations, which demonstrates the feasibility of the proposed method.

V. CONCLUSION

This paper introduced a simple scheme for synthesizing a simplified multi-segment piecewise-linear Chua's diode. The presented Chua's diode has only one extreme simple off-the-shelf electronic component-based implementation owing to employing no extra DC bias voltages and fewer components. By using the proposed Chua's diode, a Sallen-Key HPF-based Chua's circuit were further constructed to generate multi-scroll chaotic attractors. By means of mathematical model, the equilibrium points were derived and their stabilities were analyzed. The numerical simulations, circuit simulations and hardware experiments verified the feasibility of the proposed scheme. The number of scrolls can be easily adjusted as the system parameters can be systematically set. Theoretically, N -scroll chaotic attractors can be generated from the designed circuit. Moreover, the proposed multi-scroll Chua's circuit is extreme simple, inductor-free, and fully autonomous without external forcing.

REFERENCES

- [1] L. O. Chua, M. Komuro, and T. Matsumoto, "The double scroll family," *IEEE Trans. Circuits Syst. -I*, vol. 33, no. 11, pp. 1072–1118, Nov. 1986.
- [2] L. Fortuna, M. Frasca, and M. G. Xibilia, *Chua's Circuit Implementations: Yesterday, Today and Tomorrow*. Singapore: World Scientific, 2009.
- [3] A. Elwakil and M. Kennedy, "A semi-systematic procedure for producing chaos from sinusoidal oscillators using diode-inductor and fet-capacitor composites," *IEEE Trans. Circuits Syst. -I*, vol. 47, no. 4, pp. 582–590, Apr. 2000.
- [4] M. Yalçin, J. Suykens, and J. Vandewalle, "True random bit generation from a double-scroll attractor," *IEEE Trans. Circuits Syst. -I*, vol. 51, no. 7, pp. 1395–1404, Jul. 2004.
- [5] C. Shen, S. Yu, J. Lü, and G. Chen, "A systematic methodology for constructing hyperchaotic systems with multiple positive Lyapunov exponents and circuit implementation," *IEEE Trans. Circuits Syst. -I*, vol. 61, no. 3, pp. 854–864, Mar. 2014.
- [6] H. Jia, Z. Chen, and G. Qi, "Chaotic characteristics analysis and circuit implementation for a fractional-order system," *IEEE Trans. Circuits Syst. -I*, vol. 61, no. 3, pp. 845–853, Mar. 2014.
- [7] S. Vaidyanathan and C. Volos, *Advances and Applications in Chaotic Systems*. Berlin, Heidelberg, Germany: Springer, 2016.
- [8] Z. Hua, F. Jin, B. Xu, and H. Huang, "2D logistic-sine-coupling map for image encryption," *Signal Processing*, vol. 149, pp. 148–161, 2018.
- [9] Z. Hua, B. Zhou, and Y. Zhou, "Sine chaotification model for enhancing chaos and its hardware implementation," *IEEE Trans. Ind. Electron.*, vol. 66, no. 2, pp. 1273–1284, 2019.
- [10] C. Li, D. Lin, J. Lü, and F. Hao, "Cryptanalyzing an image encryption algorithm based on autoblocking and electrocardiography," *IEEE MultiMedia*, vol. 25, no. 4, 2018.
- [11] Q. Wang, S. Yu, C. Li, J. Lü, X. Fang, C. Guyeux, and J. M. Bahi, "Theoretical design and FPGA-based implementation of higher-dimensional digital chaotic systems," *IEEE Trans. Circuits Syst. -I*, vol. 63, no. 3, pp. 401–412, Mar. 2016.
- [12] Z. Hua, S. Yi, Y. Zhou, C. Li, and Y. Wu, "Designing hyperchaotic cat maps with any desired number of positive lyapunov exponents," *IEEE Trans. Cybernetics*, vol. 48, no. 2, pp. 463–473, Feb. 2018.
- [13] J. Lü and G. Chen, "Generating multiscroll chaotic attractor: theories, methods and applications," *Int. J. Bifurcation Chaos*, vol. 16, no. 04, pp. 775–858, Apr. 2006.
- [14] A. S. Elwakil, S. Özoğuz, and M. P. Kennedy, "Creation of a complex butterfly attractor using a novel lorenz-type system," *IEEE Trans. Circuits Syst. -I*, vol. 49, no. 4, pp. 527–530, Apr. 2002.
- [15] A. S. Elwakil and M. P. Kennedy, "A four-wing butterfly attractor from a fully autonomous system," *Int. J. Bifurcation Chaos*, vol. 13, no. 10, pp. 3093–3098, 2003.
- [16] G. Qi, G. Chen, S. Li, and Y. Zhang, "Four-wing attractors: from pseudo to real," *Int. J. Bifurcation Chaos*, vol. 16, no. 04, pp. 859–885, 2006.

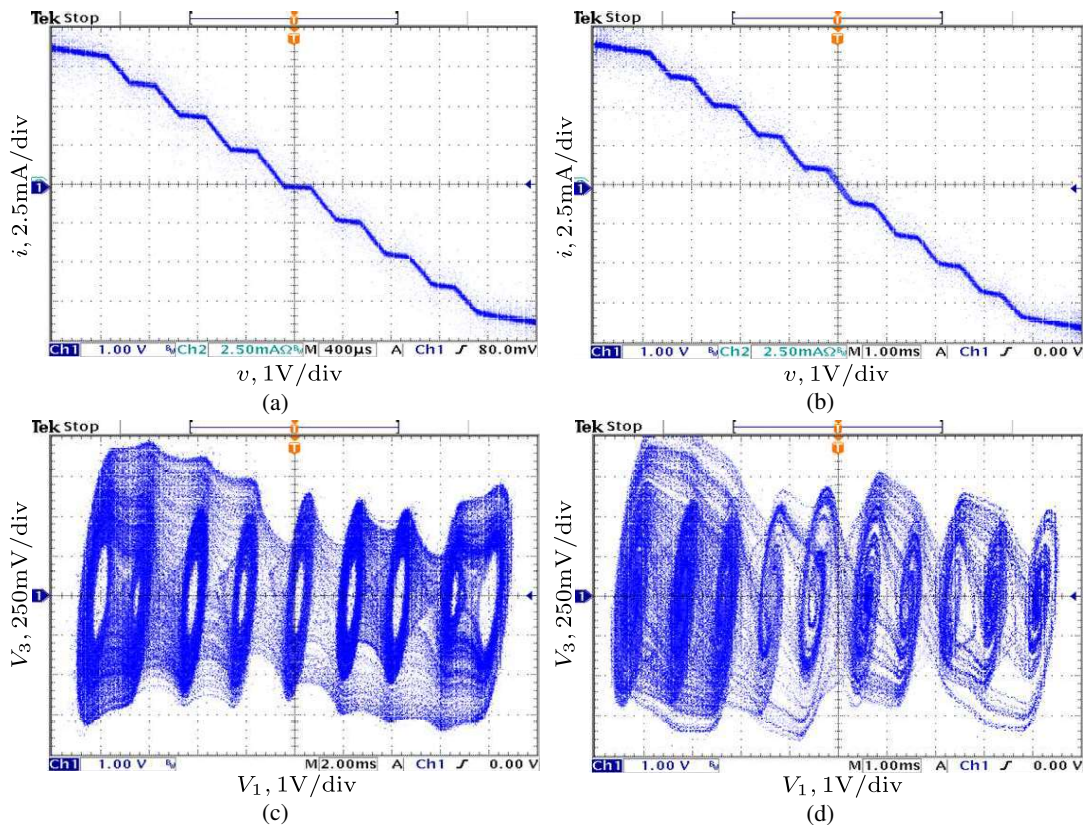


Fig. 12: Experimental results: (a) the 17-segment piecewise-linear curve; (b) the 19-segment piecewise-linear curve; (c) The 9-scroll chaotic attractor; (d) The 10-scroll chaotic attractor.

- [17] C. Volos, J. O. Maaita, S. Vaidyanathan, V. T. Pham, I. Stouboulos, and I. Kyrianiadis, "A novel four-dimensional hyperchaotic four-wing system with a saddlefocus equilibrium," *IEEE Trans. Circuits Syst. -II Exp. Briefs*, vol. 64, no. 3, pp. 339–343, Mar. 2017.
- [18] S. Yu, W. K. S. Tang, J. Lü, and G. Chen, "Generation of $n \times m$ -wing Lorenz-like attractors from a modified ShimizuMorioka model," *IEEE Trans. Circuits Syst. -II Exp. Briefs*, vol. 55, no. 11, pp. 1168–1172, Nov. 2008.
- [19] Y. Huang, P. Zhang, and W. Zhao, "Novel grid multiwing butterfly chaotic attractors and their circuit design," *IEEE Trans. Circuits Syst. -II Exp. Briefs*, vol. 62, no. 5, pp. 496–500, May. 2015.
- [20] F. R. Tahir, R. S. Ali, V. T. Pham, A. Buscarino, M. Frasca, and L. Fortuna, "A novel 4D autonomous $2n$ -butterfly wing chaotic attractor," *Nonlinear Dyn.*, vol. 85, no. 4, pp. 2665–2671, Sep. 2016.
- [21] Q. Hong, Y. Li, X. Wang, and Z. Zeng, "A versatile pulse control method to generate arbitrary multi-direction multi-butterfly chaotic attractors," *IEEE Trans. Computer-Aided Design of Integrated Circuits and Systems*, pp. 1–1, Jul. 2018.
- [22] S. Yu, J. Lü, X. Yu, and G. Chen, "Design and implementation of grid multiwing hyperchaotic Lorenz system family via switching control and constructing super-heteroclinic loops," *IEEE Trans. Circuits Syst. -I*, vol. 59, no. 5, pp. 1015–1028, May. 2012.
- [23] L. Zhou, C. Wang, and L. Zhou, "Generating hyperchaotic multi-wing attractor in a 4D memristive circuit," *Nonlinear Dyn.*, vol. 85, no. 4, pp. 1–11, Sep. 2016.
- [24] —, "A novel no-equilibrium hyperchaotic multi-wing system via introducing memristor," *Int. J. Circuit Theory Appl.*, vol. 46, no. 2, 2017.
- [25] J. A. K. Suykens and J. Vandewalle, "Quasilinear approach to nonlinear systems and the design of n -double scroll ($n = 1, 2, 3, 4, \dots$)," *IEE Proc. G*, vol. 138, no. 5, pp. 595–603, Oct. 1991.
- [26] —, "Generation of n -double scrolls ($n=1, 2, 3, 4, \dots$)," *IEEE Trans. Circuits Syst. -I*, vol. 40, no. 11, pp. 861–867, Nov. 1993.
- [27] J. A. K. Suykens, A. Huang, and L. O. Chua, "A family of n -scroll attractors from a generalized Chua's circuit," *Int. J. Electron. Commun.*, vol. 51, no. 3, pp. 131–138, 1997.
- [28] M. Yalçın, J. Suykens, and J. Vandewalle, "Experimental confirmation of 3- and 5-scroll attractors from a generalized Chua's circuit," *IEEE Trans. Circuits Syst. -I*, vol. 47, no. 3, pp. 425–429, Mar. 2000.
- [29] W. K. S. Tang, G. Zhong, G. Chen, and K. F. Man, "Generation of n -scroll attractors via sine function," *IEEE Trans. Circuits Syst. -I*, vol. 48, no. 11, pp. 1369–1372, Nov. 2001.
- [30] G. Zhong, K. F. Man, and G. Chen, "A systematic approach to generating n -scroll attractors," *Int. J. Bifurcation Chaos*, vol. 12, no. 12, pp. 2907–2915, Dec. 2002.
- [31] S. Yu, S. Qiu, and Q. Lin, "New results of study on generating multiple-scroll chaotic attractors," *Sci. China Ser. F*, vol. 46, no. 2, pp. 104–115, Feb. 2003.
- [32] S. Yu, W. K. S. Tang, and G. Chen, "Generation of $n \times m$ -scroll attractors under a Chua-circuit framework," *Int. J. Bifurcation Chaos*, vol. 17, no. 11, pp. 3951–3964, 2007.
- [33] Q. Hong, Q. Xie, and P. Xiao, "A novel approach for generating multi-direction multi-double-scroll attractors," *Nonlinear Dyn.*, vol. 87, no. 2, pp. 1015–1030, Jan. 2017.
- [34] C. Wang, X. Liu, and H. Xia, "Multi-pieces quadratic nonlinearity memristor and its $2N$ -scroll and $2N+1$ -scroll chaotic attractors system," *Chaos*, vol. 27, no. 3, p. 033114, Mar. 2017.
- [35] K. Rajagopal, S. Çiçek, P. Naseradinmousavi, A. J. M. Khalaf, S. Jafari, and A. Karthikeyan, "A novel parametrically controlled multi-scroll chaotic attractor along with electronic circuit design," *Eur. Phys. J. Plus*, vol. 133, no. 354, Sep. 2018.
- [36] N. Wang, B. Bao, Q. Xu, M. Chen, and P. Wu, "Emerging multi-double-scroll attractor from variable-boostable chaotic system excited by multi-level pulse," *IET Journal of Engineering*, vol. 1, no. 1, pp. 42–44, Jan. 2018.
- [37] L. A. B. Tôrres and L. A. Aguirre, "Inductorless Chua's circuit," *Electron. Lett.*, vol. 36, no. 23, pp. 1915–1916, Nov. 2000.
- [38] R. Rocha and R. O. Medrano-T, "An inductor-free realization of the Chua's circuit based on electronic analogy," *Nonlinear Dyn.*, vol. 56, no. 4, pp. 389–400, Jun. 2009.
- [39] O. Morgül, "Inductorless realisation of Chua oscillator," *Electron. Lett.*, vol. 31, no. 17, pp. 1403–1404, Aug. 2002.

- [40] T. Banerjee, "Single amplifier biquad based inductor-free Chua's circuit," *Nonlinear Dyn.*, vol. 68, no. 4, pp. 565–573, Jun. 2012.
- [41] B. Bao, N. Wang, M. Chen, Q. Xu, and J. Wang, "Inductor-free simplified Chua's circuit only using two-op-amp-based realization," *Nonlinear Dyn.*, vol. 84, no. 2, pp. 511–525, Apr. 2016.
- [42] B. Bao, Q. Li, N. Wang, and Q. Xu, "Multistability in Chua's circuit with two stable node-foci," *Chaos*, vol. 26, no. 4, p. 043111, Apr. 2016.
- [43] B. Bao, P. Jiang, Q. Xu, and M. Chen, "Hidden attractors in a practical Chua's circuit based on a modified Chua's diode," *Electron. Lett.*, vol. 52, no. 1, pp. 23–25, Jan. 2015.
- [44] M. E. Van Valkenburg, *Analog filter design*. Holt, Rinehart, and Winston, 1982.
- [45] B. Bao, P. Wu, H. Bao, M. Chen, and Q. Xu, "Chaotic bursting in memristive diode bridge-coupled Sallen-Key lowpass filter," *Electron. Lett.*, vol. 53, no. 16, pp. 1104–1105, Aug. 2017.
- [46] C. P. Silva, "Shil'nikov's theorem-a tutorial," *IEEE Trans. Circuits Syst.* -I, vol. 40, no. 10, pp. 675–682, Oct. 1993.
- [47] A. Wolf, J. B. Swift, H. L. Swinney, and J. A. Vastano, "Determining Lyapunov exponents from a time series," *Physica D*, vol. 16, no. 3, pp. 285–317, Jul. 1985.
- [48] B. Bao, H. Bao, N. Wang, M. Chen, and Q. Xu, "Hidden extreme multistability in memristive hyperchaotic system," *Chaos Solit. Fractals*, vol. 94, pp. 102–111, Jan. 2017.
- [49] H. Bao, N. Wang, B. Bao, M. Chen, P. Jin, and G. Wang, "Initial condition-dependent dynamics and transient period in memristor-based hypogenetic jerk system with four line equilibria," *Commun. Nonlinear Sci. Numer. Simul.*, vol. 57, pp. 264–275, Apr. 2018.